Powder Technology 448 (2024) 120231

Contents lists available at ScienceDirect

Powder Technology

journal homepage: www.journals.elsevier.com/powder-technology

The sensitivity of powder characterization tool measurements to particle properties

B.D. Jenkins [a,b,*], A.L. Nicuşan [a], A. Neveu [b], G. Lumay [c], F. Francqui [b], J.P.K. Seville [a], D. Weston [a], D. Werner [a], C.R.K. Windows-Yule [a]

[a] School of Chemical Engineering, the University of Birmingham, Edgbaston, Birmingham, B15 2TT, UK
[b] Granutools, Rue Jean Lambert Defrêne 107, 4340 Awans, Belgium
[c] Grasp laboratory, CESAM research unit, University of Liège, Place du 20 Août 7, 4000 Liège, Belgium

HIGHLIGHTS

- Rolling friction and cohesive energy density have the most influence on the bulk measurements.
- The sensitivity to frictional parameters increases with rotation rate in the rotating drum.
- The coefficient of restitution typically has the smallest influence on bulk measurements.
- An alternative bulk measurement has the potential to determine the coefficient of restitution.

GRAPHICAL ABSTRACT

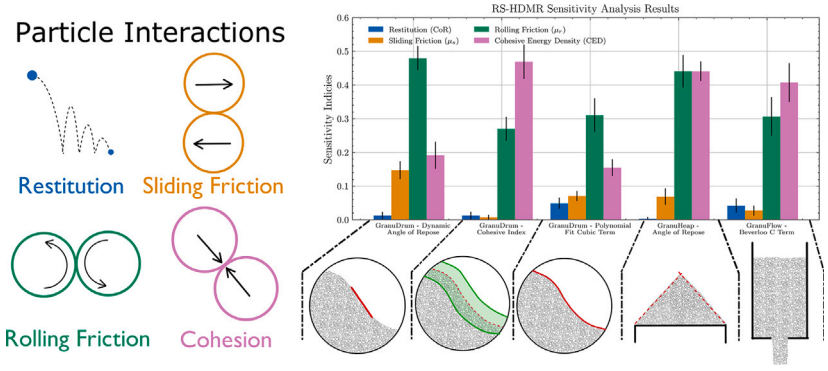

ARTICLE INFO

Keywords:
DEM simulation
Calibration
Powder characterisation
Sensitivity analysis
Particle properties

ABSTRACT

Calibration of Discrete Element Method (DEM) simulations is challenging and non-standardised. A common approach involves deducing particle properties from bulk measurements obtained through powder characterisation instruments. However, choosing the best bulk measurements for calibrating DEM simulations depends on the specific material and system. This paper presents a detailed sensitivity analysis of four commonly used bulk measurements to aid in selecting the best measurements for DEM calibration: Beverloo C fitting term (flowing density), angle of repose, dynamic angle of repose, and cohesive index. Rolling friction and cohesion significantly impact these measurements, with systems showing higher sensitivity to frictional properties in faster flow conditions, while the coefficient of restitution has low sensitivity. The cubic term of a polynomial fit to the free surface of a rotating drum was investigated for measuring the coefficient of restitution. This method demonstrated better sensitivity, particularly at lower rotational speeds.

1. Introduction

For accurate simulation of the behaviour of granular materials in experimental systems using Discrete Element Method (DEM) simulations, accurate calibration of microscopic particle properties is essential [1–4]. These properties are crucial as DEM computes the resulting normal and tangential forces on each particle contact using contact models which depend on specific coefficients to define their strength. The bulk behaviour of a material depends on many particle properties and the combination of interactions between these properties which makes finding the correct unique solution difficult. If a single bulk

* Corresponding author at: School of Chemical Engineering, the University of Birmingham, Edgbaston, Birmingham, B15 2TT, UK.
E-mail address: bdj746@student.bham.ac.uk (B.D. Jenkins).

https://doi.org/10.1016/j.powtec.2024.120231
Received 7 March 2024; Received in revised form 28 August 2024; Accepted 30 August 2024
Available online 2 September 2024

measurement is employed to calibrate multiple DEM parameters, there is often no unique solution.

Measuring these particle properties directly is challenging. Although theoretically straightforward, various factors usually render direct measurement unfeasible [1]. A more effective, albeit less direct, method involves inferring particle properties from bulk measurements, commonly known as the indirect calibration method. In this method, particle properties in a simulation are adjusted until the bulk measurement aligns with that of an experiment. For instance, the DEM particle properties in an angle of repose simulation can be adjusted until the results match the experimental angle of repose [1].

Bulk measurements have been widely utilised in numerous prior studies to determine DEM particle properties via the indirect calibration method. Peréz et al. [5] and Ajmal et al. [6] used the draw down bulk flow test to calibrate DEM simulations. Hu et al. [7] used a rotating drum and Frankowski and Morgeneyer [8] used a rotating drum in combination with a translational shear tester for DEM calibration. The well-known Hall flow test has been simulated by Dai et al. [9] to calibrate frictional and cohesive DEM particle properties of Inconel 718. Combining many bulk measurements tests together has also been used to improve the accuracy of the indirect calibration method [10]. There is no existing literature indicating which bulk measurement or combination of measurements is optimal for the indirect calibration method. However, it is obvious that a bulk measurement that is highly sensitive to a given particle property is more effective for calibrating that property.

2. Method

To determine the sensitivity of bulk measurements to particle properties, it is necessary to quantify the output variation in response to changes in the input. Sensitivity analysis, a data analysis technique, can be used to analyse a large dataset and extract quantitative information on output variation due to input variation. This quantitative information is extracted in the form of sensitivity indices.

To use sensitivity analysis to find the sensitivity of bulk measurements to particle properties, a data set containing particle properties as variables and bulk measurements as the measured outputs is required. For accurate analysis, the dataset must encompass all realistic values of the particle properties. However, generating such a comprehensive data set through experiments is impractical. Therefore, Discrete Element Method (DEM) simulations of powder characterisation instruments and their bulk measurements are utilised.

2.1. Powder characterisation instruments and bulk measurements

The powder characterisation instruments chosen for this sensitivity study include a rotating drum [11,12], a flow-through-an-orifice tester, and an angle of repose tester [13]. The specific instruments used are the Granutools GranuDrum (rotating drum), GranuHeap (angle of repose tester), and GranuFlow (flow-through-an-orifice tester). These instruments were selected because they represent a standardised method for powder characterization widely adopted in both academia and industry.

The bulk measurements investigated are: the Beverloo C fitting term (or flowing density), the angle of repose, the dynamic angle of repose, the cohesive index, and a polynomial fit to the free surface. A summary of the bulk measurements along with the associated powder characterisation instrument is presented in Table 1.

Table 1
Summary of the characterisation instruments and the relevant bulk measurements for each instrument.

Characterisation instrument	Bulk measurements
Angle of repose tester	Angle of repose
Flow through an orifice tester	Flow rate through an orifice
Rotating drum	Dynamic angle of repose
	Cohesive index
	3rd order polynomial cubic ‘a’ term

2.2. DEM simulations

Conducting experiments to collect the necessary data is impractical because of the challenges of creating powders with precisely defined (and precisely measurable) particle properties and the time-intensive nature of experimental procedures. DEM has been utilised to solve both issues.

The DEM software PICI-LIGGGHTS [14] was chosen, which is a modified version of the open-source LIGGGHTS software [15], itself based on the molecular dynamics simulator LAMMPS [16]. PICI-LIGGGHTS was selected due to being open-source, and the integrated Python wrapper that enables dynamic updates of simulations and parameters. This flexibility enables the automated launch of mass-scale simulations, with more than 1000 simulations running simultaneously on the University of Birmingham BlueBear HPC and the University of Warwick Sulis Tier 2 HPC facilities.

By using DEM simulation, the microscopic properties of powder grains can be precisely defined, allowing the inputs of the data set to be precisely set. Individual particle-level information, such as positions and velocities, can be extracted and used to faithfully replicate the analysis used for the experimental bulk measurement techniques. Precisely replicating the geometry, operation, and bulk measurements of powder characterization instruments within the DEM simulations results in the creation of the powder characterisation digital twins described in Section 3 that are needed to generate the data. These open-source digital twins can be found on GitHub: https://github.com/uob-positron-imaging-centre/DigitalTwins and GitLab: https://gitlab.com/gdigitaltwins/.

The Hertz–Mindlin contact model [17,18] was used in the DEM simulations to calculate the normal and tangential forces on the particles, energy dissipation due to the coefficient of restitution and the implementation of the sliding friction coefficient (μ_s). The constant directional torque (CDT) model [19] was used for the rolling friction (μ_r) and the simplified Johnson-Kendall-Roberts (SJKR) model [6] for inter-particle cohesive forces via the cohesive energy density (CED) coefficient. The contact law equations can be found in Appendix A.

2.3. Sensitivity analysis techniques

Previous work on the sensitivity of bulk measurements to particle properties is sparse. Yan et al. [20] used three levels of sensitivity analysis to look at the sensitivity of flow rate through an orifice and angle of repose to the Young’s Modulus, coefficient of restitution and static and rolling friction coefficients. However, they only considered two bulk measurement techniques and did not include cohesive forces in the study, which have a considerable influence on the behaviours of powders.

The sensitivity analysis method used in this paper is: Random Sampling High-Dimensional Model Representation (RS-HDMR). More details on the fundamentals of RS-HDMR will be presented in Section 4. To validate the findings of RS-HDMR, the approach of employing principal component analysis (PCA) in the second level of sensitivity analysis, as utilized by Yan et al. [20], can be similarly applied to the dataset. The full explanation of the method implemented and results from the PCA sensitivity analysis can be found in the supplementary material.

Table 2
Summary of the microscopic particle properties considered in this sensitivity analysis study.

Microscopic particle properties	Particle property values tested
Coefficient of Restitution (CoR)	0.1, 0.5, 0.9
Sliding friction (μ_s)	0.15, 0.2, 0.3, 0.5, 0.8, 1.0
Rolling friction (μ_r)	0.01, 0.05, 0.1, 0.2, 0.4, 0.7
Cohesive Energy Density (CED)	0, 10 000, 20 000, 30 000, 40 000, 50 000, 70 000

2.4. Data collection

Both RS-HDMR and PCA require a large dataset of system inputs and outputs. For this study, a dataset is required where the input DEM particle properties are varied, and the bulk measurement outputs from each powder characterisation instrument digital twin are recorded.

A minimum of several hundred data points (typically $N > 300$) is required for reliable RS-HDMR results [21]. For PCA, the commonly cited minimum sample sizes range from 150 to 300, with 500 or more being considered very good [22–24]. Due to the use of DEM simulations of the powder characterisation instruments in this study, sample sizes considerably exceed 500, typically ranging from 800 to 1000, ensuring a robust dataset.

The bulk measurements and particle properties considered are summarized in Tables 1 and 2 respectively. Choosing the range of values for this study was non-trivial, as many particle properties do not have a maximum value. The coefficient of restitution is the only property with a maximum value of 1, while sliding friction, rolling friction, and cohesive energy density have a minimum of 0 but no set maximum. Cohesive energy density refers to the cohesion strength per unit volume (J/m^3) in the Simplified-JKR (SJKR) contact model [25].

All simulations were conducted with an average particle diameter of 1.1 mm with a log-normal particle size distribution (Fig. B.16 in Appendix B shows the full distribution), a Poisson's ratio of 0.3, and an intrinsic density of 1000 kg/m^3. These parameters were chosen based on their relevance to real granular materials. For example, microcrystalline cellulose has a Poisson's ratio of 0.3, and aspirin crystals have a value of 0.29 [26]. An intrinsic density of 1000 kg/m^3 falls within the range of many pharmaceutical and chemical materials commonly tested using characterization instruments.

In total, 5880 simulations were run with unique combinations of the coefficient of restitution, sliding friction, rolling friction, and cohesive energy density across the three DEM digital twins (including three different rotation speeds in the rotating drum). Bulk measurements were recorded for use in the sensitivity analysis, with the same values for each particle property applied to all digital twins to provide the best comparison between them.

2.5. Superquadric particles

Real particles often have restricted rotation due to the non-spherical shape of the particles themselves. Modelling such particles in DEM is typically too computationally expensive to do compared to spherical particles so the effect of restricted rotation is sometimes simulated using a rotational resistance or rolling friction model [19]. To contextualize the influence of rolling friction, superquadric particles have been used to find the non-spherical particle shape that has an equivalent bulk behaviour to different coefficients of rolling friction. The results of this are presented in Section 5.6.4.

The geometry of a superquadric particle is described by the formula: $f(x) = (|\frac{x}{a}|^{n_2} + |\frac{y}{b}|^{n_2})^{n_1/n_2} + |\frac{z}{c}|^{n_1} - 1 = 0$, where a, b, and c represent the half lengths of the particle, and n_1 and n_2 are parameters determining the blockiness [27]. In this study, $n_1 = n_2 = 2$ was used to form ellipsoids. The dimensions a, b, and c were adjusted so that $b = c$ and $a = AR * b$, with AR being the aspect ratio. To maintain a consistent volume across particles with varying aspect ratios, a, b, and c were scaled to ensure volume equivalence for any aspect ratio as well as being equivalent in volume to the spherical particles.

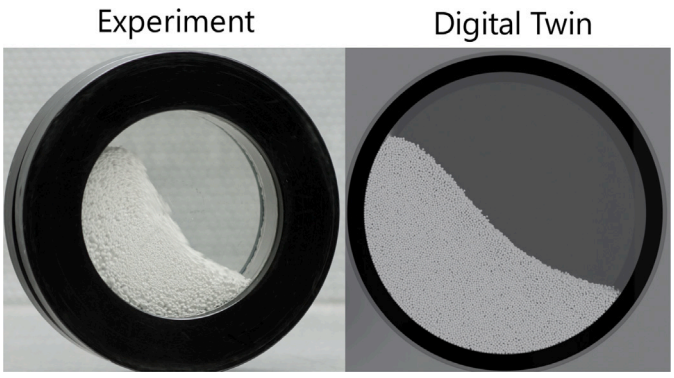

Fig. 1. Rotating drum instrument on the left and digital twin on the right.

3. Powder characterisation instrument digital twins

3.1. Rotating drum - GranuDrum

Both the physical rotating drum instrument and the digital twin consist of a cylinder that rotates around a central axis like a wheel. The cylinder has an internal diameter of 8.4 cm and a depth of 2 cm and is filled with 50 ml of powder, which is approximately 45% of the total volume of the drum. The rotation speed can vary between 2–60 RPM. Images of the drum and powder are taken at a plane perpendicular to the axis of rotation (such that the drum is a circle) every second over 50 s. The full details and development of the digital twin of the rotating drum (GranuDrum) will be published in a future paper.

Fig. 1 shows the rotating drum instrument and digital twin. Three bulk measurements are considered: two widely used measurements, the dynamic angle of repose and the cohesive index, along with an alternative measurement, a polynomial fit to the powder free surface.

The dynamic angle of repose is a measurement widely used in rotating drums that involves measuring the average angle of the material flowing in the drum. The cohesive index is calculated from an image of $x \times y$ pixels taking the y pixel value of the powder-air interface of the powder at every x position and calculating the standard deviation between the position of y at each x pixel over 50 images taken 1 s apart. The complete details of the dynamic angle of repose and cohesive index measurement have been published by Neveu et al. [28].

Fig. 2 illustrates a diagram of the images used to measure the bulk flow properties in the rotating drum. A section of the image around the edge of the drum is cropped to exclude particles that might have stuck to the drum wall from the bulk flow measurements analysis. This cropped section is also excluded during bulk measurement analysis in the digital twin of the rotating drum to maintain accuracy relative to the actual instrument.

A polynomial fit is a refinement of fitting a single dynamic angle of repose. Fig. 2 shows a diagram of the comparison between these two measurements. Instead of fitting an angle to the free surface, a third-order polynomial of the form $y = ax^3 + bx^2 + cx + d$ is fitted to the free surface, where x and y are the pixel values of the free surface interface. From fitting this polynomial, the values for a, b, c and d can be recorded.

Applying a polynomial fit to the free surface of a material in a rotating drum is not a new idea. Orpe and Khakhar [29] employed a tenth-order polynomial, while Prasad and Khakhar [30] used a sixth-order polynomial. However, this method is not yet widely used in powder characterisation.

Each of the a, b, c, and d terms could be used as bulk measurements of the material because they define the shape of a 3rd order polynomial which approximates the free surface shape, which is dependent on particle properties. However, only the a term will be investigated in this study as explained in the next paragraph.

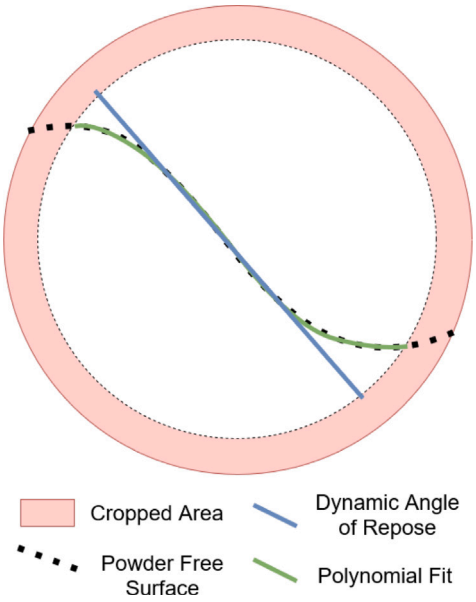

Fig. 2. Comparison of the dynamic angle of repose and the polynomial fit.

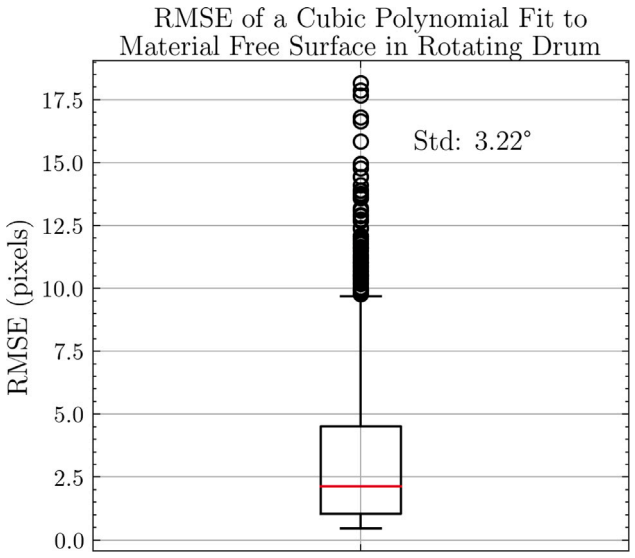

Fig. 3. RMSE error between the y pixel values of the actual interface coordinates and the cubic polynomial fit.

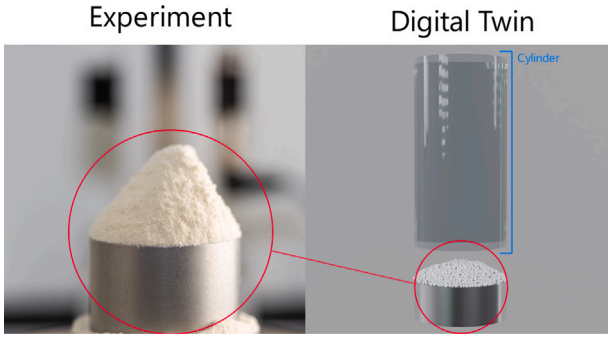

Fig. 4. Angle of repose tester instrument on the left and digital twin on the right.

The cubic a coefficient of the polynomial is shown to have a higher sensitivity to the coefficient of restitution. This is important as no powder characterisation instrument is currently available that measures the coefficient of restitution, and the other measurements tested in this paper were not sensitive to the coefficient of restitution, as will be discussed in Section 5. There will be slight variability in all these measurements as they are based on image analysis, so the exact value will vary depending on the set of images used. An example of the expected variability has been shown in Section 3.2 for the angle of repose tester.

To show the suitability of the cubic polynomial fit for a powder free surface in a rotating drum over a wide range of particle properties, Fig. 3 shows a box plot of the root mean square error (RMSE) between y position of the average interface extracted from the images and the y position predicted by a cubic polynomial fit for the same average interface in all simulations of the rotating drum of 30 RPM. The mean RMSE was around 2 pixels (0.42 mm) between the polynomial and the actual interface values showcasing that in most cases the polynomial fit can capture the shape of the free surface well. However, there are some outliers with the most egregious having a RMSE of 18 pixels, equivalent to 3.78 mm. These outliers were for simulations that had a combination of large particle cohesion forces and high frictions.

3.2. Angle of repose tester - GranuHeap

Fig. 4 illustrates both the experiment and the digital twin of the angle of repose tester. The full details and development of the angle of repose tester (GranuHeap) used here will be published in a future paper.

The physical instrument and digital twin use the cylinder lifting method to form a heap. In this method, a hollow cylinder with an inner diameter of 4 cm is placed on top of a cylindrical base with an outer diameter of 4 cm such that no particles can escape. The cylinder is filled with the material to be measured. Once the fill level in the cylinder reaches a predetermined amount, it is raised at a constant rate and the material forms a heap below it, as shown. After the cylinder is no longer in contact with the material and the material has stabilized, the angle of the heap can be measured.

The measurement of the angle of repose in the digital twin has been implemented to be identical to the procedure in the experimental instrument. An image of the heap is taken in a horizontal plane such that the heap resembles a triangle shape. The angle of repose is then computed by finding the area equivalent isosceles triangle to the material in the image. This is then repeated a number of times (typically 16) while rotating the heap so that each image is of a unique side of the heap. The average angle measured for all the images is then used to compute an average angle of repose [31].

As in the rotating drum there will be slight variation in the data. This is due to random variation in the insertion of the particles initially causing the measurement to slightly vary. To quantify this, 20 simulations were run, 10 with very low friction and cohesive energy density values and 10 with higher friction and cohesive energy density values. Each of the 20 simulations used different random 'seed' values to insert the particles to create completely random particle insertions but keeping everything else the same. The variability in these simulations can then be visualised using two box plots in Fig. 5. These box plots show that the variation is very low between each simulation with the low friction and cohesion case having a standard deviation of 0.03 degrees and the higher friction and cohesion case having a standard deviation of 0.27 degrees.

3.3. Flow through an orifice - GranuFlow

A digital twin of the flow through an orifice, mass flow rate tester (GranuFlow) was developed to complement the previously existing digital twins of the rotating drum and angle of repose tester. The full

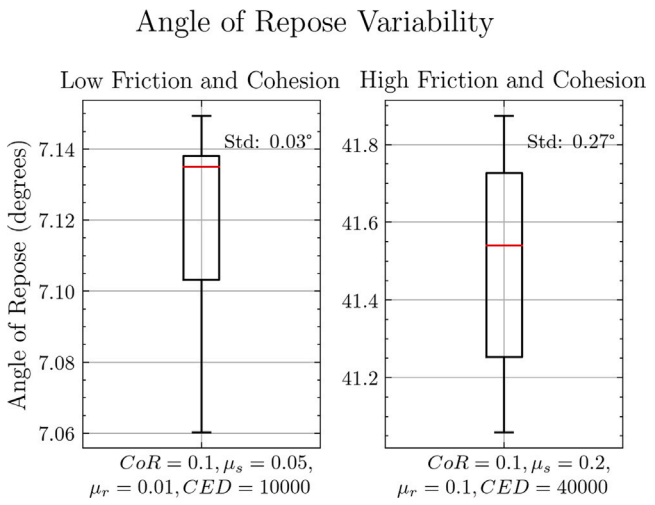

Fig. 5. Variation of values in the angle of repose tester digital twin for two different sets of DEM particle properties. On the left the particle properties are: $CoR = 0.1, \mu_s = 0.05, \mu_r = 0.01, CED = 10000$. On the right the particle properties are: $CoR = 0.1, \mu_s = 0.2, \mu_r = 0.1, CED = 40000$.

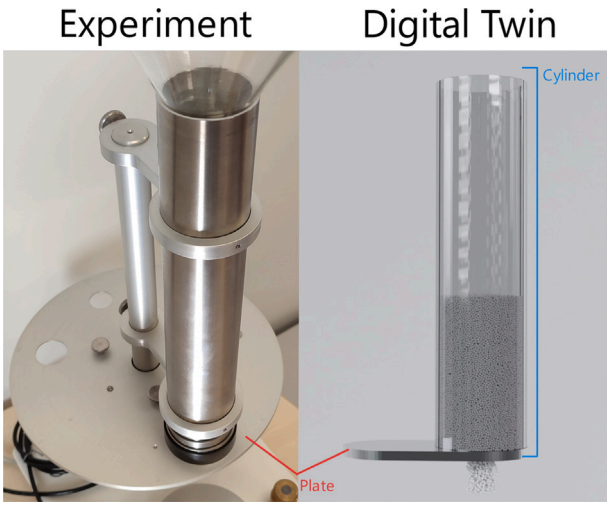

Fig. 6. Flow through an orifice instrument on the left and digital twin on the right.

details of the flow through an orifice digital twin and its development will be published in a future paper.

Fig. 6 shows the digital twin next to the lab instrument. The geometry of the mass flow rate tester is a flat bottomed silo. To operate it, a cylinder with an internal diameter of 4.75 cm is filled with the powder being tested while the bottom is closed. Then a plate with an orifice of a certain diameter is slid underneath the cylinder so that the orifice is in the centre of the cylinder. Powder flows through and collects on an electronic mass scale until discharge is complete, giving a measurement of the mass flow rate.

The mass flow rate in the DEM simulation can differ slightly depending on the initial arrangement of the particles during the filling process. This variation occurs because the particles are randomly generated at the top of the tube and then allowed to settle under gravity to achieve a random packing configuration. An example of the expected variability has been shown in Section 3.2 for the angle of repose tester.

The digital twin used the same geometry and orifice sizes as in the experiment: 2, 4, 8, 12, 18, 22, 28 mm. The Beverloo equation, first developed by Beverloo et al. [32,33], as in Eq. (1) can be fitted to the data for the mass flow rate vs orifice size data.

$$W = c\rho\sqrt{g}(d_0 - kd)^{\frac{5}{2}} \tag{1}$$

where W is the mass flow rate, c is a fitting parameter related to the properties of the granular material, ρ is the bulk density of the material, g is acceleration due to gravity, d_0 is the diameter of the orifice for a given flow rate, k is another fitting parameter related to how particles flow near the edge of the orifice and d is the average particle diameter.

The GranuFlow uses a modified implementation of the Beverloo equation, as in Eq. (2), where the c fitting term and ρ are combined into the C fitting term and kd is combined into the D_{min} term.

$$W = C\sqrt{g}(d_0 - D_{min})^{\frac{5}{2}} \tag{2}$$

where C is a fitting parameter related to the properties of the granular material and D_{min} is a fitting parameter relating to the minimum orifice diameter at which flow occurs. The sensitivity results investigate the sensitivity to the C term, the small c term, and the flowing density ρ_f.

4. Sensitivity analysis methodology

Many sensitivity analysis techniques are available for analysing large data sets and are split into two main groups: local sensitivity analysis and global sensitivity analysis.

Local sensitivity analysis, which relies on derivatives, evaluates the sensitivity of outputs to small perturbations in inputs. While effective for linear systems, it is less informative for non-linear systems or those with unknown linearity. Derivatives offer information only around the evaluation point, not the full parameter space [34,35]. Common local sensitivity techniques include adjoint sensitivity analysis and Green's function method [36]. Since the linearity of the data is not known, local sensitivity analysis may give misleading results.

Global Sensitivity Analysis (GSA) ranks the importance of system inputs based on their impact on output variance. Saltelli et al. [37] define GSA as "the study of how the uncertainty in the output of a model (numerical or otherwise) can be apportioned to different sources of uncertainty in the model input". Unlike local sensitivity, GSA explores the entire parameter space, providing a robust measure of sensitivity, accommodating nonlinearity and complex interactions between inputs [38,39].

The GSA technique, high dimensional model representation (HDMR), initially explored by Rabitz et al. [40] was chosen for this study due to its flexibility. Unlike other global sensitivity methods such as Sobol sensitivity analysis [41] and the Morris method [42,43], HDMR does not require a specific input sampling method. This allows it to be used with uncontrolled lab data or computationally expensive simulation data as in this work [38]. Specifically, the Random Sampling HDMR (RS-HDMR) method developed by Li et al. [38] is employed.

The next sections provide a brief overview of global sensitivity analysis and RS-HDMR, but for comprehensive details of the methodologies, refer to Li et al. [38] and additional resources on HDMR global sensitivity analysis [44–46].

4.1. Global sensitivity analysis general form

Global sensitivity analysis expresses the relationship between the system inputs and outputs in a similar way to the decomposition of $f(x)$ as in the general form, Eq. (3) [38].

$$y = f(x) = f_0 + \sum_{i=1}^{n} f_i(x_i) + \sum_{1\le i<j\le n} f_{ij}(x_i, x_j) + \cdots + f_{1,2,\ldots,n}(x_1, x_2, \ldots, x_n) \tag{3}$$

where y and $f(x)$ are the outputs of the system and the terms on the right are the component functions for 1 to n interactions. f_0 is the mean response of the whole model, $\sum_{i=1}^{n} f_i(x_i)$ are the first-order component functions, and $\sum_{1\le i<j\le n} f_{ij}(x_i, x_j)$ are the second-order component functions.

Component functions may extend up to the order n, corresponding to the number of inputs. The final term on the right is an error between

the best approximation of all the component functions and the actual output value. For HDMR analysis to be more effective, it is beneficial if higher-order component functions are considered to have minimal impact on the final output [38,47].

Finding the exact solutions to the component functions is difficult. Instead, RS-HDMR (Random Sampling High-Dimensional Model Representation) approximates component functions as orthonormal polynomials or splines [38,47]. The implementation of RS-HDMR by Li et al. [38] approximates the component functions as cubic B splines defined by:

$$f_i(x_i) \approx \sum_{r=-1}^{m+1} \alpha_r^i B_r(x_i) \tag{4}$$

$$f_{ij}(x_i, x_j) \approx \sum_{p=-1}^{m+1} \sum_{q=-1}^{m+1} \beta_{pq}^{ij} B_p(x_i) B_q(x_j) \tag{5}$$

where m is the number of knots, $B_{r,p,q}(x_{i,j})$ are the cubic B splines and, α_r^i and β_{pq}^{ij} are constants that need to be ascertained [38].

Substituting these into Eq. (3) gives an additive model. A backfitting algorithm fits this model to the data [38]. Sensitivity indices are then calculated for each component function using:

$$S_{p_j} = Cov(f_{p_j}, Y)/V(Y) \approx \sum_{s=1}^{N} f_{p_j}(\boldsymbol{X}_{p_j}^{(s)})(y^{(s)} - \overline{y})/\sum_{s=1}^{N}(y^{(s)} - \overline{y})^2 \tag{6}$$

$$S_{p_j}^a = Var(f_{p_j})/V(Y) \approx \sum_{s=1}^{N}(f_{p_j}(\boldsymbol{X}_{p_j}^{(s)}))^2/\sum_{s=1}^{N}(y^{(s)} - \overline{y})^2 \tag{7}$$

$$S_{p_j}^b = S_{p_j} - S_{p_j}^a \tag{8}$$

where S_{p_j} is the total sensitivity, $S_{p_j}^a$ is the structural sensitivity, $S_{p_j}^b$ is the correlative sensitivity, Cov is the covariance, Y is the generic aspect of the output y (i.e. a representative example value from all of the output values), N is the total number of samples, $\boldsymbol{X}$ is a vector of input variables x, $y^{(s)}$ is all the output variables in the sample from 1 to N, $\overline{y}$ is the mean of all values in $y^{(s)}$.

4.2. Precise form

Saltelli et al. [37] provide an introductory example using the Ishigami function [48].

The application of RS-HDMR to study the influence of particle properties on bulk measurements involves input $x_1 = CoR, x_2 = \mu_s, x_3 = \mu_r, x_4 = CED$ and a bulk measurement output y. Third order and higher component functions were neglected in this paper meaning the specific form of Eq. (3) only includes interactions up to the second order:

$$\begin{aligned} y = f(x) = {} & f_0 + f_1(x_1) + f_2(x_2) + f_3(x_3) + f_4(x_4) + \\ & f_{12}(x_1, x_2) + f_{13}(x_1, x_3) + f_{14}(x_1, x_4) + f_{23}(x_2, x_3) + \\ & f_{24}(x_2, x_4) + f_{34}(x_3, x_4) + f_{1,2,3,4}(x_1, x_2, x_3, x_4) \end{aligned} \tag{9}$$

The component functions are estimated using cubic B splines and estimated through backfitting [38]. Sensitivity indices are calculated for each component function using the equations provided in (6)–(8).

4.3. Practical implementation

The RS-HDMR approach is implemented in Python using the SALib library [49]. The data must be arranged into a matrix with a shape $N \times d$, where N is the number of samples, and d is the number of particle properties. A problem specification is generated, and the sensitivity analysis is repeated for each bulk measurement. The output is a set of first and second-order sensitivity indices for each particle parameter and their combinations that sum to one, though only the first order will be considered in the results [38,49].

In this study, with particles measuring an average diameter of 1.1 mm, each digital twin (comprising the rotating drum, angle of repose tester, and flow through an orifice tester) has N combination. This is equivalent to the total unique particle property combinations displayed in Table 2. Specifically, $N = 3 \times 6 \times 6 \times 7 = 756$. Additionally, the rotating drum was simulated at three different rotational speeds, leading to a total of 3780 simulations analysed across all three digital twins. $d = 4$ corresponds to the four variable particle properties.

5. Results

The first order sensitivity indices from the RS-HDMR sensitivity analysis are shown in Fig. 7. The black lines indicate the 95% confidence interval for each of the sensitivity indices. The confidence intervals were calculated using the bootstrap method as originally proposed by Storlie et al. [21]. A higher sensitivity indicates, for a given bulk measurement, that the respective microscopic particle property is more influential, and that bulk measurement is better for calibrating that property.

Firstly, regarding the overall trends, rolling friction and cohesion show the strongest influence of all on the bulk measurements. None of the bulk measurements showed a high sensitivity to sliding friction when compared to the sensitivity to rolling friction and cohesion in the range investigated here. The coefficient of restitution is overall the least influential particle property across all the measurements, not going above a sensitivity index of around 0.05.

5.1. Dynamic angle of repose - GranuDrum

The dynamic angle of repose is the first measurement considered in Fig. 7. The dynamic angle of repose is associated with how challenging it is for particles to move past one another. The more difficult it is, the further the particles will move up the wall in the direction of the drum rotation, creating a steeper angle from the top-most particles to the lowest. The dynamic angle of repose is conceptually similar to the angle of repose but there are interesting differences in the sensitivity analysis.

The sensitivity to the coefficient of restitution is slightly higher in the dynamic system because of constant collisions. However, the value is still negligible compared to the other particle properties at around 0.02. The influence of cohesive energy density is reduced from 0.44 in the static angle of repose to 0.19 in the dynamic angle of repose. The higher energy state will make it easier for cohesive bonds to be broken meaning fewer particles will be in contact at any given time.

The dynamic angle of repose has a higher sensitivity to the sliding friction compared to the static angle of repose doubling from 0.07 to 0.14. Rolling friction, on the other hand, has a similar large influence on the dynamic angle of repose as the static angle of repose, with an index of 0.47. This indicates that rolling friction is independent of how dynamic a system is.

5.2. Cohesive index sensitivity - GranuDrum

The cohesive index is a bulk measurement that was developed to measure the cohesive forces in a powder by analysing the fluctuations in the powder free surface caused by transient clumping of particles. Neveu et al. [28] detail the exact methodology for calculating the cohesive index.

The sensitivity analysis in Fig. 7 shows that, as expected, the cohesive energy density has by far the strongest influence on the cohesive index, with a sensitivity index of 0.47. This is twice as high as rolling friction, which has a sensitivity index of around 0.26 and more than twenty times higher than the coefficient of restitution.

As with all previous bulk measurements, the coefficient of restitution shows little influence with a sensitivity index around 0.02. The sliding friction also has a negligible effect on the cohesive index measurement with a sensitivity index of essentially 0.

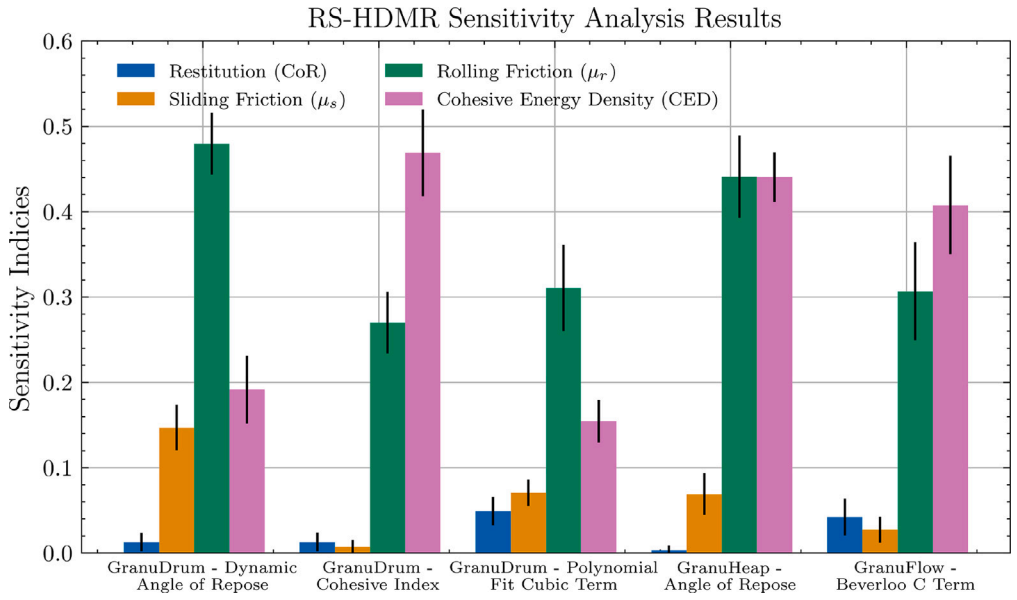

Fig. 7. Bar graph of the sensitivity indices for the dynamic angle of repose, cohesive index and polynomial cubic 'a' term, the angle of repose and C fitting parameter in the Beverloo equation in relation to each of the four microscopic particle properties investigated.

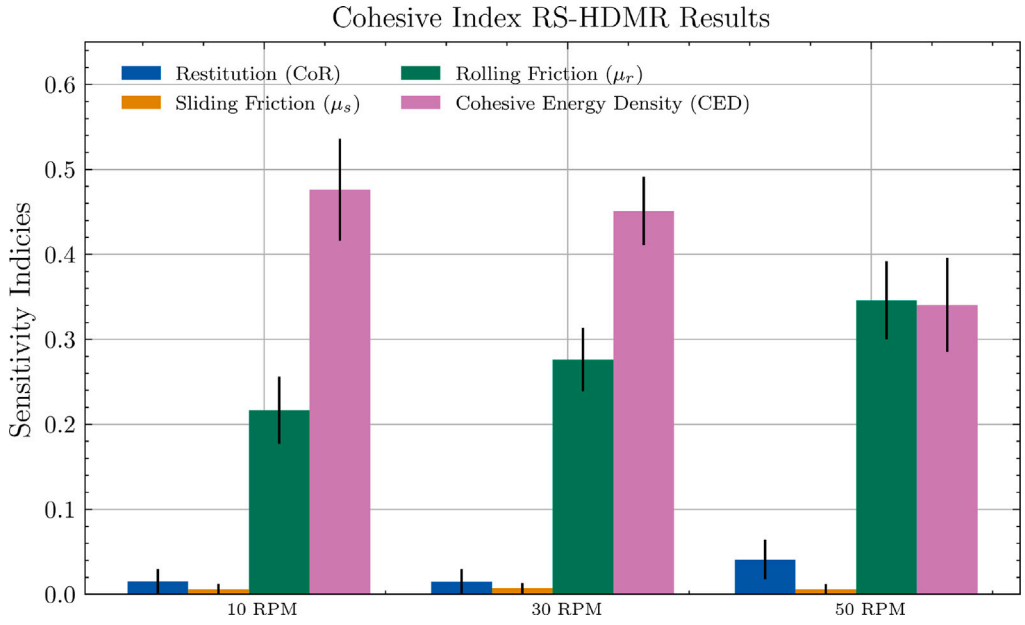

Fig. 8. The sensitivity indices of the cohesive index measurement in the GranuDrum digital twin at different rotational speeds in the rotating drum.

5.3. Angle of repose - GranuHeap

In the fourth measurement shown in Fig. 7, the angle of repose obtained from the angle of repose tester (GranuHeap) digital twin indicates that rolling friction and cohesion are once again the most significant particle properties. Each had an equal significance with both showing a sensitivity index around 0.44.

The angle of repose is essentially the largest angle that a stable pile can form. The stronger the forces acting to prevent particles from moving past each other the higher the stable angle that can be achieved. Cohesion, sliding friction, and rolling friction should all act to prevent particles from moving past or away from each other. This explains why rolling friction and cohesive energy density have high sensitivity indices. Sliding friction, however, has a much lower sensitivity compared to cohesive forces and rolling friction with an index of around 0.07.

The angle of repose is a static measurement, so the coefficient of restitution is not expected to have any influence because there are no collisions. The results confirm this as they show the coefficient of restitution having a sensitivity index of essentially 0.

5.4. Beverloo equation - GranuFlow

The bulk measurement on the right of Fig. 7 is the fitting parameter C in the Beverloo equation previously discussed in Section 3.3.

Cohesive energy density and rolling friction have the largest influence on the C fitting term with sensitivity indices of 0.41 and 0.31 respectively. Since the particles are confined, contact density is high, so cohesion significantly impacts this bulk measurement. However, high values of the cohesive energy density frequently led to no mass flow through the orifice. Consequently, using an orifice tester to

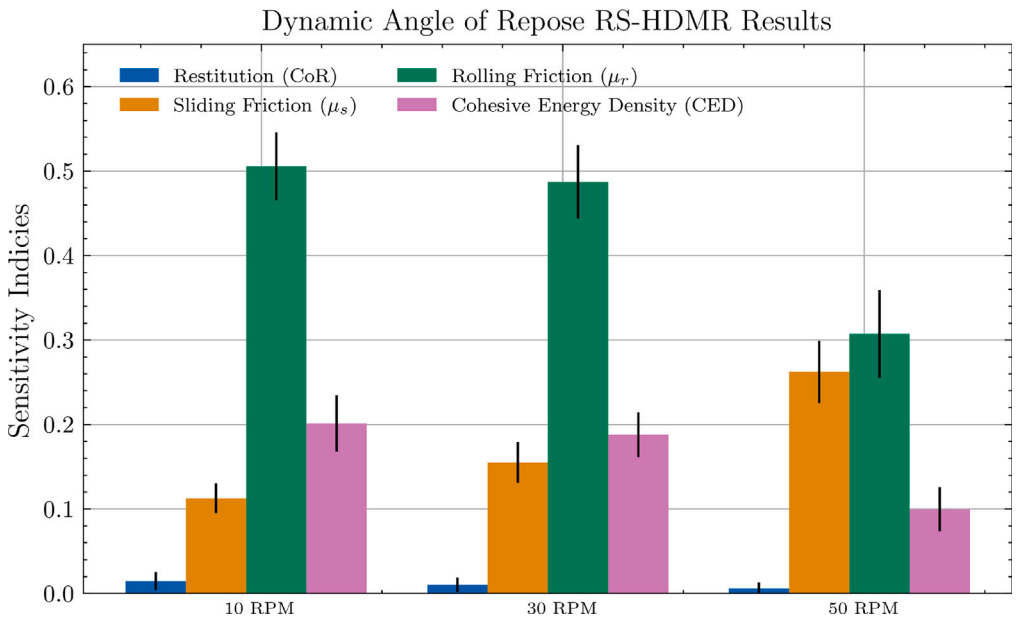

Fig. 9. The sensitivity indices of the dynamic angle of repose measurement in the GranuDrum digital twin at different rotational speeds.

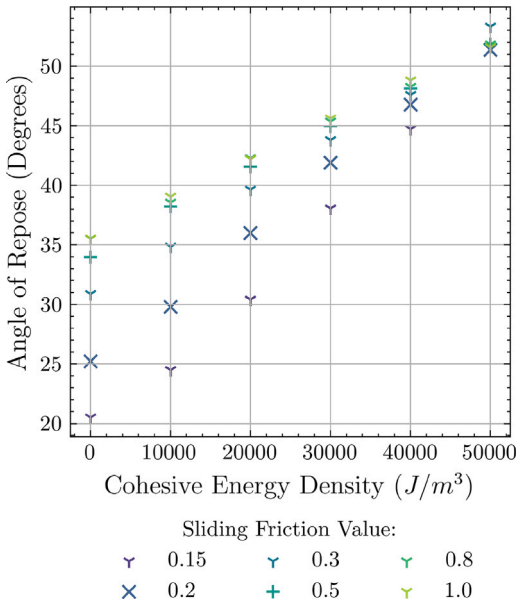

Fig. 10. The angle of repose in the GranuHeap digital twin versus cohesive energy density for $\mu_s = 0.15 - 1.0$ at $\mu_r = 0.2$ and $CoR = 0.5$.

study highly cohesive powders is often ineffective because obtaining a reliable measurement is challenging in many instances.

The sensitivity to sliding friction is small compared to rolling friction and cohesion, with a sensitivity index of around 0.025. This is perhaps unintuitive as the particles should slide past each other when flowing downward. This could be explained by the previously discussed saturation effect observed in sliding friction for the angle of repose or the fact that rolling friction and cohesion are more significant. For flow to occur the material needs to dilate and dilation is caused by particle rearrangement which in turn is strongly linked to rotation of particles [50]. Since rolling friction impacts particle rotation this could also explain the strong influence of rolling friction.

The sensitivity of the result to the coefficient of restitution is small compared to rolling friction and cohesion, with an index of around 0.04. Due to the nature of the confined system, there are very few energetic collisions and thus the coefficient of restitution does not have a large impact on the measurement.

5.5. Polynomial fit cubic term - GranuDrum

None of the previous bulk measurements have shown a strong sensitivity to the coefficient of restitution. This leads to the question of whether a bulk measurement technique exists that is sensitive to this particle property.

The sensitivity of the cubic a term of the polynomial to the coefficient of restitution is shown in the middle of Fig. 7 and shows a small increase in the value of the sensitivity index compared to the Beverloo C term. The value increased from around 0.04 to 0.05. Rolling friction and cohesion are still the most influential particle properties. However, this bulk measurement technique shows potential to extend the range of use of the rotating drum to the measurement of the coefficient of restitution. Further investigation into the effect of rotation rate on sensitivity is presented in Section 5.6.6.

5.6. Further investigation

5.6.1. GranuDrum cohesive index - effect of rotation rate

The effect of rotation rate on the cohesive index measurement was investigated. Fig. 8 shows the results for the cohesive index at 10, 30 and 50 RPM.

The cohesive index shows no change in the sensitivity to sliding friction no matter what rotational speed is used. A steady upward trend in rolling friction sensitivity as rotational speed increases can be seen, ranging from 0.23 at 10 RPM to 0.34 at 50 RPM. The coefficient of restitution remains insignificant except at 50 rpm where it increases to 0.04.

5.6.2. GranuDrum dynamic angle of repose - effect of rotation rate

Fig. 9 shows the sensitivity of the dynamic angle of repose to particle properties at 10, 30, and 50 RPM.

The most obvious trend is the increase of the influence of sliding friction from a sensitivity index of 0.12 at 10 RPM to 0.26 at 50 RPM. This shows that at faster material flow sliding friction has more of an influence. Rolling friction here shows a decrease in sensitivity going from 0.51 at 10 RPM to 0.30 at 50 RPM. However, this may be due to the increasing sensitivity to sliding friction causing rolling friction

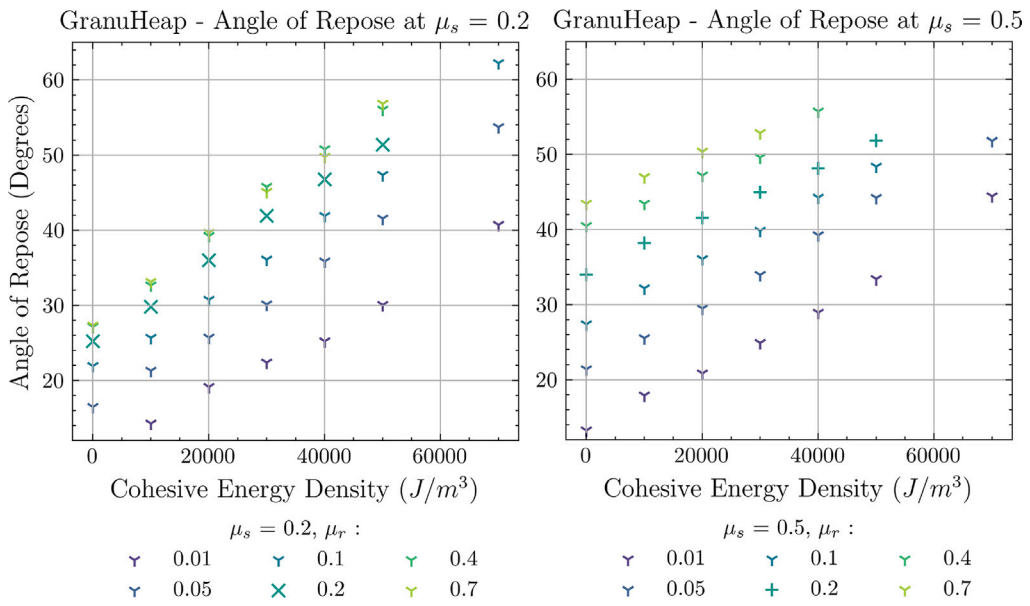

Fig. 11. The angle of repose in the GranuHeap digital twin versus cohesive energy density for $\mu_r = 0.01 - 0.7$ at $CoR = 0.5$. The graph on the left has $\mu_s = 0.2$ and on the right a value of $\mu_s = 0.5$.

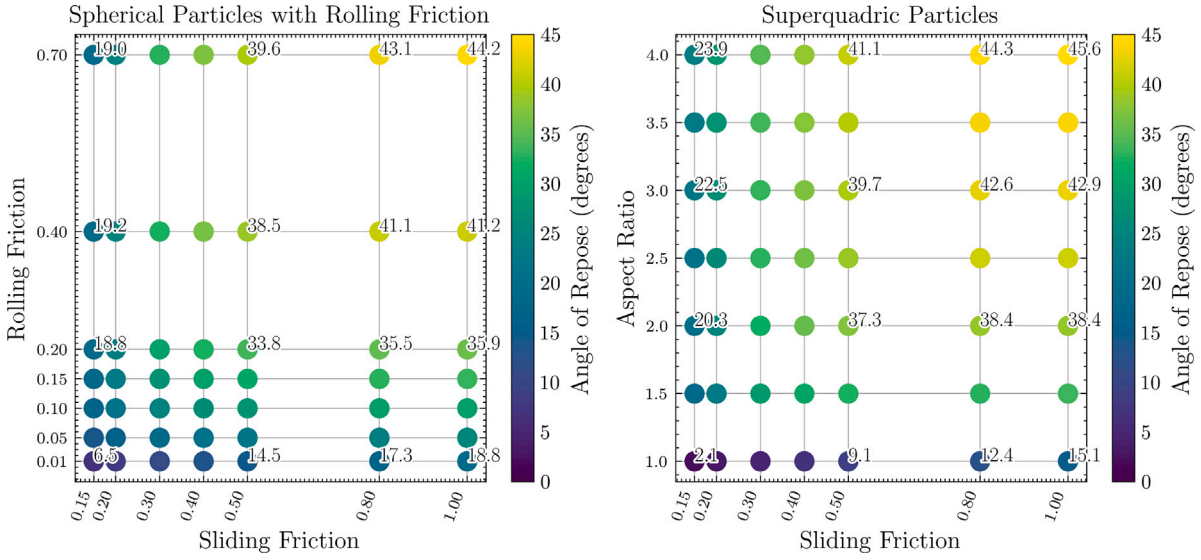

Fig. 12. On the left, the measured angle of repose in the GranuHeap digital twin of spherical particles with rolling friction. On the right, the measured angle of repose in the GranuHeap digital twin of elliptical particles with $\mu_r = 0$. For both, $CoR = 0.5$ and $CED = 20000$.

to appear like it is less sensitive. Cohesive energy density appears to show a slight decreasing sensitivity with increasing rotation rate but the effect of the coefficient of restitution remains negligible at all rotation rates.

5.6.3. GranuHeap - investigation into sliding and rolling friction

Yan et al. [20] conducted a sensitivity analysis on a different angle of repose tester and identified a saturation effect of sliding friction. Yan's results indicated that sliding friction had the greatest impact on bulk responses between $\mu_s = 0.05$ and $\mu_s = 0.25$, with a diminished effect from $\mu_s = 0.25$ to $\mu_s = 0.5$. This suggests a non-linear relationship where increasing sliding friction beyond a certain point no longer affects the bulk response. This saturation effect is reproduced in the present study and is described in the next paragraph.

Fig. 10 illustrates the angle of repose measured in the angle of repose digital twin at $\mu_r = 0.2$ and $CoR = 0.5$. At zero cohesive energy density, the angle of repose increases by approximately 10.5 degrees as sliding friction rises from $\mu_s = 0.15$ to $\mu_s = 0.3$, but only by 5 degrees from $\mu_s = 0.3$ to $\mu_s = 1.0$. This trend persists across different cohesive energy densities, with lower sliding friction values showing larger changes in the angle of repose.

In contrast, rolling friction does not show the same degree of saturation in the angle of repose measured in the GranuHeap digital twin, as shown in Fig. 11. For $\mu_s = 0.5$, higher rolling friction values do not saturate, although when $\mu_s = 0.2$, there is some saturation, as indicated by the overlap angle of repose values for $\mu_r = 0.4$ and $\mu_r = 0.7$.

If μ_s values below 0.15 were considered, a higher sensitivity to sliding friction would probably be observed in the bulk measurements. However, a lower limit of 0.15 was chosen because values lower than this made measurements impossible due to changes in regimes of material flow. For example, at high values of cohesive energy density and $\mu_s < 0.15$ the material in the rotating drum digital twin would tend to stay as one solid body and slide against the wall in a slumping regime.

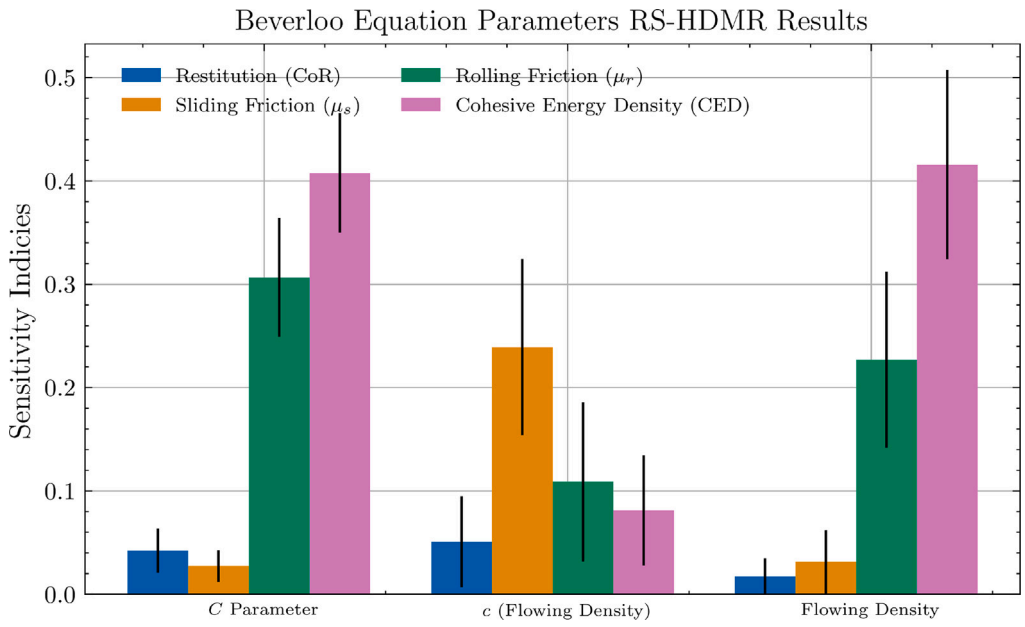

Fig. 13. RS-HDMR sensitivity results for some of the parameters used in the Beverloo equation.

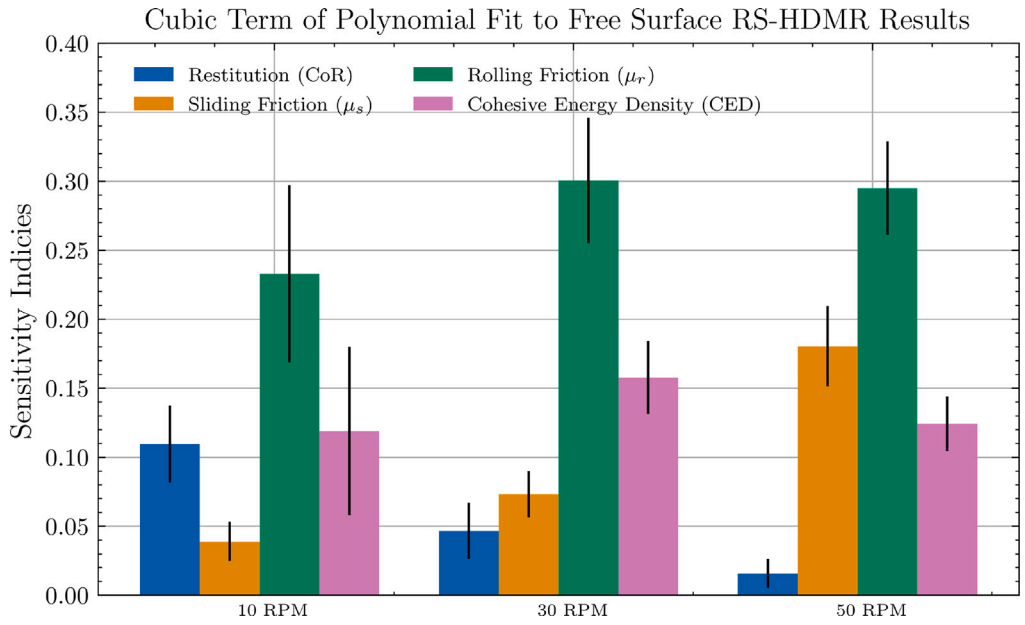

Fig. 14. Global RS-HDMR sensitivity analysis results for the polynomial fit to the free surface in the rotating drum powder characterisation instrument for different drum rotation speeds.

This form of behaviour prevents useful measurements of dynamic angle of repose or cohesive index.

5.6.4. GranuHeap - comparison of rolling friction to elliptical particles

As Fig. 7 shows, rolling friction significantly influences all bulk measurements. To give context to the strong effect that rolling friction has on all measurements, the effect of rolling friction on the angle of repose can be compared to a physical change in the particle shape. Rolling friction resists particle rotation and is often used in DEM to reproduce the resistance due to rolling of non-spherical particles [51–53].

Fig. 12 compares the angle of repose in the GranuHeap digital twin for elliptical superquadric particles with $\mu_r = 0$ and spherical particles with $\mu_r = 0.01 - 0.7$. The left graph shows that the angle of repose for spherical particles with $\mu_s = 1$ and $\mu_r = 0.7$ closely matches that of elliptical particles with $\mu_s = 1$ and an aspect ratio of 4. A value of 0.7 for the rolling friction has a similar effect on the angle of repose as physically changing the shape of a particle to have an aspect ratio of 4.

Additionally, the angle of repose shows minimal variation for $\mu_r > 0.15$ when $\mu_s < 0.3$, ranging between approximately 18.8° and 20°. For $\mu_r = 0.01 - 0.2$, the angle of repose changes from 6.5° to 18.8° given the same sliding friction (μ_s). When the sliding friction μ_s is ≥ 0.3, the influence of rolling friction on the angle of repose becomes more significant, suggesting an interaction between sliding and rolling friction. For instance, at $\mu_s = 1.0$, with μ_r varying from 0.01 to 0.2, the angle of repose ranges from 18.8° to 35.9°.

The elliptic superquadric particles displayed similarly interesting behaviour, with only a minor influence on the angle of repose observed between particle aspect ratios of $AR = 2 - 4$, where the measured angle varied from 20.3° to 23.9°. In contrast, the shift in measured angle was

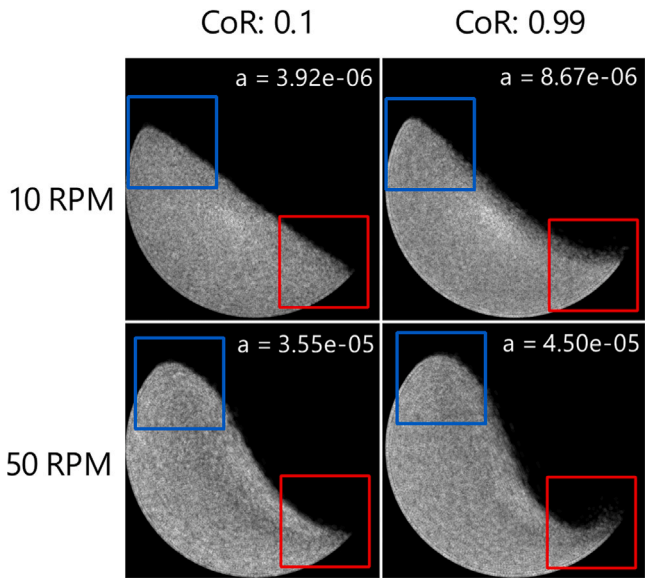

Fig. 15. Different free surface shapes in a DEM simulation of the GranuDrum digital twin for 10 and 50 RPM and $CoR = 0.1$ and $CoR = 0.99$. For all images, $\mu_s = 0.5$, $\mu_r = 0.4$ and $CED = 0$.

significant between a spherical particle and a particle with $AR = 2$, changing from 2.1° to 20.3°.

5.6.5. GranuFlow - investigation of different fitting terms

Previous researchers have used different estimates for the bulk density in the Beverloo equation, Eq. (1). Nedderman [54] recommends the choice of the flowing density (ρ_f), which is defined as the ratio of the mass flow rate to the volumetric flow, calculated from the observed rate of descent of the top surface. He reported that this reduces the observed range of c to 0.575–0.595 [55].

This study also reinforces Nedderman's results [54] by showing that the variation in the c term for the flowing density version of Beverloo's equation was much smaller, between $c = 0.54 - 0.68$, compared to the c term used with Beverloo's equation using bulk density, between $c = 0.35 - 0.65$. A further study on this will be published in the future.

To further support Nedderman's [54] claim, the sensitivity index of c can be compared to the sensitivity index of C used in the modified version of the Beverloo equation, Eq. (2). If c is truly mostly constant the sensitivity of the flowing density and C to particle properties should be similar because C is essentially the combination of c and flowing density. Fig. 13 shows the RS-HDMR sensitivity indices for the C fitting term as well as the c fitting term when used with flowing density and the flowing density measurement itself.

The similar sensitivity indices between the C term and the flowing density adds further credit to Nedderman's [54] results that the c term is essentially constant. The main difference between the two being a reduced sensitivity to rolling friction with the C term having a sensitivity index of 0.31 and the flowing density having an index of around 0.22. The c term does exhibit some dependence on the particle properties with sliding friction being the most important having a sensitivity index of 0.24.

5.6.6. GranuDrum polynomial fit - effect of rotation rate

To further investigate the sensitivity to the coefficient of restitution of this new bulk measurement, the rotating drum digital twin was run again over the same parameter range for the particle properties as outlined in Table 2, but for a slower rotation rate at 10 rpm and a higher rotation rate at 50 rpm. RS-HDMR analysis was conducted on this new data across the three rotation speeds.

Fig. 14 shows the RS-HDMR sensitivity results of the polynomial bulk measurement at the different rotational speeds. There is a clear trend of decreasing sensitivity to the coefficient of restitution as the rotational speed is increased. The 10 rpm results have the highest sensitivity to the coefficient of restitution so far with an index of 0.11.

The increase in sensitivity of the cubic term in the polynomial fit to the free surface is due to how the shape of the free surface changes with rotational speed. Fig. 15 depicts a side profile of particles in the rotating drum for two different rotational speeds and two different coefficient of restitution values, with the areas of particular interest marked by coloured boxes.

The area of interest concerning the coefficient of restitution is highlighted with a red square. Inside this red square, a higher coefficient of restitution results in a more distinct rounding of the surface as the particles collide with the drum wall. This phenomenon is partially what the cubic term measures. The other aspect, indicated by the blue boxes, is the increased surface curvature at the top as particles flow over the heap. In the 50 RPM scenario, there is already a complex, nonlinear free surface shape unlike the simpler linear shape in the 10 RPM scenario. This makes it easier to pick up the surface rounding that occurs at the tail end and does not get drowned out by the more exaggerated shape of the rest of the free surface.

Examining the cubic term a across the images in Fig. 15, it is observed that at a coefficient of restitution value of 0.1, the values are comparable for both 10 rpm and 50 rpm. However, at a coefficient of restitution value of 0.99, the value of a in the 10 rpm case is nearly twice that of the 50 rpm case, making it possible to distinguish the two cases by the shape of the flowing region alone.

Another noteworthy aspect is the heightened sensitivity to sliding friction as system dynamics increase (faster flow), as shown in Fig. 14. This suggests that a higher rotational speed is preferable when using the polynomial fit to study sliding friction, whereas a lower speed is more suitable for examining the coefficient of restitution. Although a comprehensive analysis of a bulk measurement significantly affected by the coefficient of restitution is outside the scope of this paper, it merits further investigation.

A potential improvement to this approach would be to remove the crop that is currently applied to all images. Fig. 2 illustrates that an outer ring is removed during image processing. This ring is where most of the surface rounding occurs. The purpose of this is to prevent any granular material that may have adhered to the drum wall from affecting measurements.

6. Discussion and future work

DEM requires values to be chosen as particle property inputs but methods for measuring those values on a single contact basis are problematic [1]. Bulk measurements can solve some of the problems of single contact based measurements but there is no comprehensive study of which bulk measurement should be used for which particle property input. This study is an attempt to determine which bulk measurement or sets of measurements are most influenced by different particle properties and thus which technique provides the optimal chance of calibrating a plausible value for each particle property input.

Considering all the sensitivity results, the rotating drum had the highest sensitivity to all four of the particle properties across three bulk measurements, indicating that it is the best single characterisation instrument to use for calibration. The dynamic angle of repose had the highest sensitivity to rolling and sliding friction, cohesive index the highest sensitivity to cohesive forces, and the cubic term of the polynomial fit had the highest sensitivity to the coefficient of restitution.

The rotating drum also has the advantage of being able to use different rotation speeds which changed the sensitivity values of all the bulk measurements. This led to the cubic term of the polynomial fit having an even higher sensitivity to the coefficient of restitution at

slower rotating rates. However, the rotating drum only characterises materials under dynamic conditions. Material calibration in different dynamic states may create more robust calibrated properties so using more than one instrument together may be advantageous. This is something that was not investigated in the present work but warrants further study.

Various particle properties were kept constant in this study such as: the particle density, average particle size and particle size distribution. The effect these have on the sensitivity of the bulk measurements to the particle properties was not investigated and needs further study. The sensitivity analysis of more powder characterisation instruments should also be investigated, such as a tapped density tester.

7. Conclusion

In this paper, the random sampling high dimensional model representation (RS-HDMR) sensitivity analysis technique has been used to analyse the influence of particle properties on bulk measurements in powder characterisation instruments to provide guidance on the choice of which bulk measurement is better for calibrating which particle properties in DEM simulations. This is useful information for DEM users when deciding which bulk measurement or sets of measurements should be used to calibrate simulations. To obtain the large amount of data required for RS-HDMR, 5880 total DEM simulations were run using digital twins of powder characterisation instruments.

The three bulk measurements in the rotating drum had the most evenly balanced sensitivities to the four particle properties investigated. The dynamic angle of repose had the highest sensitivity to sliding and rolling friction, the cohesive index had the highest sensitivity to cohesive energy density and the cubic term of the polynomial fit had the highest sensitivity to the coefficient of restitution. The polynomial fit in the rotating drum also offers the possibility for better calibrating the coefficient of restitution at slow rotation rates. Enhancing the image analysis by eliminating the cropping process might also lead to further improvements in sensitivity.

Based on these findings, the recommended bulk measurements for the calibration of the DEM input properties – coefficient of restitution, sliding friction, rolling friction and cohesive energy density – are the dynamic angle of repose, cohesive index, and the cubic component in a polynomial fit to the powder free surface, all of which can be obtained from rotating drum experiments.

CRediT authorship contribution statement

B.D. Jenkins: Writing – original draft, Visualization, Validation, Methodology, Investigation, Formal analysis, Data curation, Conceptualization. **A.L. Nicuşan:** Software, Methodology, Data curation, Conceptualization. **A. Neveu:** Writing – review & editing, Supervision, Conceptualization. **G. Lumay:** Writing – review & editing, Supervision, Project administration, Conceptualization. **F. Francqui:** Writing – review & editing, Project administration, Funding acquisition. **J.P.K. Seville:** Writing – review & editing, Supervision, Project administration, Conceptualization. **D. Weston:** Methodology. **D. Werner:** Software. **C.R.K. Windows-Yule:** Writing – review & editing, Supervision, Project administration, Methodology, Investigation, Funding acquisition, Conceptualization.

Declaration of competing interest

The authors declare the following financial interests/personal relationships which may be considered as potential competing interests: Ben Jenkins reports financial support was provided by Granutools. Filip Franqui reports a relationship with Granutools that includes: board membership. Geoffroy Lumay reports a relationship with Granutools that includes: board membership. Aurelien Neveu reports a relationship with Granutools that includes: employment. If there are other authors, they declare that they have no known competing financial interests or personal relationships that could have appeared to influence the work reported in this paper.

Table A.3
Parameter symbols.

Symbol	Parameter
A	Contact area
CED	Cohesive energy density
CoR	Coefficient of Restitution
E^*	Effective Young's modulus
F^n_{coh}	Cohesive force normal component
F^n_{ij}	Normal force between particles i and j
F^t_{ij}	Tangential force between particles i and j
g	Gravitational acceleration
G^*	Shear modulus
I_i	Moment of inertia of particle i
k^n	Normal stiffness coefficient
k^t	Tangential stiffness coefficient
m_i	Mass of particle i
m^*	Effective mass
μ_r	Rolling friction coefficient
μ_s	Static friction coefficient
r	Lever arm from the point of contact to the centre of mass of the particle
R^*	Effective radius of the two particles in contact
τ^r_{ij}	Rolling friction torque
v^n_{ij}	Relative normal velocity between particles i and j
v^t_{ij}	Relative tangential velocity between particles i and j
δ^n_{ij}	Normal overlap between particles i and j
δ^t_{ij}	Tangential overlap between particles i and j
$\frac{dv_i}{dt}$	Acceleration of particle i
$\frac{d\omega_i}{dt}$	Angular acceleration of particle i
ω_{ij}	Relative angular velocity between particles i and j

Data availability

Data will be made available on request.

Acknowledgements

Authors acknowledge financial support received from the Centre for Doctoral Training in Formulation Engineering (EPSRC, United Kingdom grant number EP/S023070/1) and Granutools. Computational resources have been provided by the Sulis Tier 2 HPC platform hosted by the Scientific Computing Research Technology Platform at the University of Warwick and the University of Birmingham BlueBear facility (see http://www.birmingham.ac.uk/bear for more details).

Appendix A. Dem equations of motion and contact laws

Newton's Second Laws of Motion (see Table A.3):

$$m_i \frac{dv_i}{dt} = \sum (F^n_{ij} + F^t_{ij}) + m_i g \tag{A.1}$$

$$I_i \frac{d\omega_i}{dt} = \sum (r \times F^t_{ij}) - \tau^r_{ij} \tag{A.2}$$

Hertz–Mindlin normal and tangential force between two soft-body particles:

$$F^n_{ij} = -\frac{4}{3} E^* \sqrt{R^* \delta^n_{ij}}\, \delta^n_{ij} - 2\sqrt{\frac{5}{6}} \frac{\ln(CoR)}{\sqrt{\ln^2(CoR) + \pi^2}} \sqrt{k^n m^*}\, v^n_{ij} \tag{A.3}$$

$$F^t_{ij} = \begin{cases} -8G^* \sqrt{R^* \delta^n_{ij}}\, \delta^t_{ij} - 2\sqrt{\frac{5}{6}} \frac{\ln(CoR)}{\sqrt{\ln^2(CoR)+\pi^2}} \sqrt{k^t m^*}\, v^t_{ij} & |F^t_{ij}| < \mu_s |F^n_{ij}| \\ -\mu_s |F_n| \frac{\delta^t_{ij}}{|\delta^t_{ij}|} & otherwise \end{cases} \tag{A.4}$$

Constant directional torque equation for rolling friction:

$$\tau^r_{ij} = \mu_r k^n \delta^n_{ij} \frac{\omega_{ij}}{\left|\omega_{ij}\right|} R^* \tag{A.5}$$

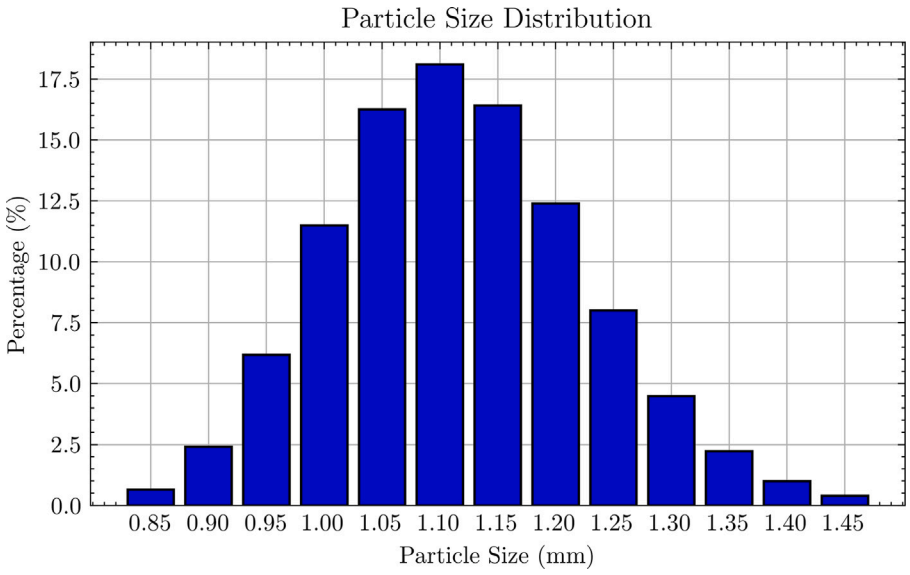

Fig. B.16. Particle size distribution used in all the simulations of this study.

Simplified-JKR cohesion model:

$$F_{coh}^{n} = CED \times A \tag{A.6}$$

Appendix B. Particle size distribution

See Fig. B.16.

Appendix C. Supplementary data

Supplementary material related to this article can be found online at https://doi.org/10.1016/j.powtec.2024.120231.

References

[1] C.R.K. Windows-Yule, A. Neveu, Calibration of DEM simulations for dynamic particulate systems, Pap. Phys. 14 (2022) http://dx.doi.org/10.4279/pip.140010, URL: https://www.papersinphysics.org/papersinphysics/article/view/795.

[2] C.R.K. Windows-Yule, D.R. Tunuguntla, D.J. Parker, Numerical modelling of granular flows: a reality check, Comput. Part. Mech. 3 (3) (2016) 311–332, http://dx.doi.org/10.1007/s40571-015-0083-2, URL: https://doi.org/10.1007/s40571-015-0083-2.

[3] W. Ketterhagen, C. Wassgren, A perspective on calibration and application of DEM models for simulation of industrial bulk powder processes, Powder Technol. 402 (2022) 117301, http://dx.doi.org/10.1016/J.POWTEC.2022.117301.

[4] C.R.K. Windows-Yule, Discrete element method modelling, in: M.J. Rhodes, J.P.K. Seville (Eds.), Introduction to Particle Technology, third ed., John Wiley & Sons, 2024, pp. 102–133.

[5] J. Marín Pérez, T. Comlekci, Y. Gorash, D. MacKenzie, Calibration of the DEM sliding friction and rolling friction parameters of a cohesionless bulk material, Particuology 92 (2024) 126–139, http://dx.doi.org/10.1016/J.PARTIC.2024.05.003.

[6] M. Ajmal, T. Roessler, C. Richter, A. Katterfeld, Calibration of cohesive DEM parameters under rapid flow conditions and low consolidation stresses, Powder Technol. 374 (2020) 22–32, http://dx.doi.org/10.1016/J.POWTEC.2020.07.017.

[7] Z. Hu, X. Liu, W. Wu, Study of the critical angles of granular material in rotary drums aimed for fast DEM model calibration, Powder Technol. 340 (2018) 563–569, http://dx.doi.org/10.1016/J.POWTEC.2018.09.065.

[8] P. Frankowski, M. Morgeneyer, Calibration and validation of DEM rolling and sliding friction coefficients in angle of repose and shear measurements, 2013, pp. 851–854, http://dx.doi.org/10.1063/1.4812065.

[9] L. Dai, Y.R. Chan, G. Vastola, N. Khan, S. Raghavan, Y.W. Zhang, Characterizing the intrinsic properties of powder – A combined discrete element analysis and hall flowmeter testing study, Adv. Powder Technol. 32 (1) (2021) 80–87, http://dx.doi.org/10.1016/J.APT.2020.11.015.

[10] T. Roessler, C. Richter, A. Katterfeld, F. Will, Development of a standard calibration procedure for the DEM parameters of cohesionless bulk materials – part I: Solving the problem of ambiguous parameter combinations, Powder Technol. 343 (2019) 803–812, http://dx.doi.org/10.1016/J.POWTEC.2018.11.034.

[11] ISO/ASTM, ISO/ASTM TR 52952:2023 Additive Manufacturing of Metals — Feedstock Materials — Correlating of Rotating Drum Measurement with Powder Spreadability in PBF-LB machines, Tech. Rep., ISO, 2023.

[12] T.A. Poole, Apparatus for determining powder flowability, 1999, United States Patent and Trademark Office, Patent Number: US5959222A.

[13] O.D. Neikov, D.V. Lotsko, V.G. Gopienko, Powder characterization and testing, Handb. Non-Ferrous Met. Powders: Technol. Appl. (2009) 7–44, http://dx.doi.org/10.1016/B978-1-85617-422-0.00001-X.

[14] University of Birmingham Positron Imaging Centre, UoB positron imaging centre's improved LIGGGHTS distribution - PICI-LIGGGHTS-3.8.1, 2022, URL: https://github.com/uob-positron-imaging-centre/PICI-LIGGGHTS.

[15] C. Kloss, C. Goniva, A. König, S. Amberger, S. Pirker, Models, algorithms and validation for opensource DEM and CFD-DEM, Prog. Comput. Fluid Dyn. 12 (2012) 140–152, http://dx.doi.org/10.1504/PCFD.2012.047457.

[16] A.P. Thompson, H.M. Aktulga, R. Berger, D.S. Bolintineanu, W.M. Brown, P.S. Crozier, P.J. in 't Veld, A. Kohlmeyer, S.G. Moore, T.D. Nguyen, R. Shan, M.J. Stevens, J. Tranchida, C. Trott, S.J. Plimpton, LAMMPS - a flexible simulation tool for particle-based materials modeling at the atomic, meso, and continuum scales, Comput. Phys. Comm. 271 (2022) 108171, http://dx.doi.org/10.1016/J.CPC.2021.108171.

[17] C.J. Coetzee, Review: Calibration of the discrete element method, Powder Technol. 310 (2017) 104–142.

[18] R.D. Mindlin, H. Deresiewicz, Elastic spheres in contact under varying oblique forces, J. Appl. Mech. (1953) 327–344, http://dx.doi.org/10.1115/1.4010702.

[19] J. Ai, J.F. Chen, J.M. Rotter, J.Y. Ooi, Assessment of rolling resistance models in discrete element simulations, Powder Technol. 206 (3) (2011) 269–282, http://dx.doi.org/10.1016/J.POWTEC.2010.09.030.

[20] Z. Yan, S.K. Wilkinson, E.H. Stitt, M. Marigo, Discrete element modelling (DEM) input parameters: understanding their impact on model predictions using statistical analysis, Comput. Part. Mech. 2 (3) (2015) 283–299, http://dx.doi.org/10.1007/s40571-015-0056-5.

[21] C.B. Storlie, L.P. Swiler, J.C. Helton, C.J. Sallaberry, Implementation and evaluation of nonparametric regression procedures for sensitivity analysis of computationally demanding models - ScienceDirect, 2009, URL: https://www.sciencedirect.com/science/article/pii/S0951832009001112?via=ihub.

[22] A.L. Comrey, H.B. Lee, A First Course in Factor Analysis, Psychology Press, 1992, http://dx.doi.org/10.4324/9781315827506.

[23] R.B. Cattell, The Scientific Use of Factor Analysis in Behavioral and Life Sciences, Springer US, Boston, MA, 1978, http://dx.doi.org/10.1007/978-1-4684-2262-7.

[24] G. Hutcheson, N. Sofroniou, The Multivariate Social Scientist, SAGE Publications, Ltd., 6 Bonhill Street, London EC2A 4PU, 1999, http://dx.doi.org/10.4135/9780857028075.

[25] C. Coetzee, O.C. Scheffler, Comparing particle shape representations and contact models for DEM simulation of bulk cohesive behaviour, Comput. Geotech. 159 (2023) 105449, http://dx.doi.org/10.1016/J.COMPGEO.2023.105449.
[26] R. Roberts, R. Rowe, P. York, The Poisson's ratio of microcrystalline cellulose, Int. J. Pharm. 105 (2) (1994) 177–180, http://dx.doi.org/10.1016/0378-5173(94)90463-4.
[27] A. Podlozhnyuk, S. Pirker, C. Kloss, Efficient implementation of superquadric particles in Discrete Element Method within an open-source framework, Comput. Part. Mech. 4 (1) (2017) 101–118, http://dx.doi.org/10.1007/s40571-016-0131-6.
[28] A. Neveu, F. Francqui, G. Lumay, Measuring powder flow properties in a rotating drum, Measurement (2022) 111548, http://dx.doi.org/10.1016/j.measurement.2022.111548, URL: https://www.sciencedirect.com/science/article/pii/S0263224122007655.
[29] A.V. Orpe, D.V. Khakhar, Scaling relations for granular flow in quasi-two-dimensional rotating cylinders, Phys. Rev. E 64 (3) (2001) 031302, http://dx.doi.org/10.1103/PhysRevE.64.031302.
[30] D.V.N. Prasad, D.V. Khakhar, Granular flow in rotating cylinders with noncircular cross sections, Phys. Rev. E 77 (4) (2008) 041301, http://dx.doi.org/10.1103/PhysRevE.77.041301.
[31] G. Lumay, F. Boschini, K. Traina, S. Bontempi, J.C. Remy, R. Cloots, N. Vandewalle, Measuring the flowing properties of powders and grains, Powder Technol. 224 (2012) 19–27, http://dx.doi.org/10.1016/J.POWTEC.2012.02.015.
[32] W.A. Beverloo, H.A. Leniger, J.v.d. Velde, The flow of granular solids through orifices, Chem. Eng. Sci. 15 (3–4) (1961) 260–269.
[33] J.P.K. Seville, U. Tüzün, R. Clift, Processing of Particulate Solids, Blackie Academic & Professional, London, 1996.
[34] J. Morio, Global and local sensitivity analysis methods for a physical system, Eur. J. Phys. 32 (6) (2011) 1577–1583, http://dx.doi.org/10.1088/0143-0807/32/6/011.
[35] A. Saltelli, M. Ratto, T. Andres, F. Campolongo, J. Cariboni, D. Gatelli, M. Saisana, S. Tarantola, Sensitivity analysis: From theory to practice, in: Global Sensitivity Analysis. The Primer, John Wiley & Sons, Ltd, 2007, pp. 237–275, http://dx.doi.org/10.1002/9780470725184.ch6, URL: https://onlinelibrary.wiley.com/doi/abs/10.1002/9780470725184.ch6.
[36] X. Zhou, H. Lin, Local sensitivity analysis, in: Encyclopedia of GIS, Springer US, Boston, MA, 2008, p. 616, http://dx.doi.org/10.1007/978-0-387-35973-1{_}703.
[37] A. Saltelli, S. Tarantola, F. Campolongo, M. Ratto, Sensitivity Analysis in Practice, Wiley, 2002, http://dx.doi.org/10.1002/0470870958.
[38] G. Li, H. Rabitz, P.E. Yelvington, O.O. Oluwole, F. Bacon, C.E. Kolb, J. Schoendorf, Global sensitivity analysis for systems with independent and/or correlated inputs, Procedia - Soc. Behav. Sci. 2 (6) (2010) 7587–7589, http://dx.doi.org/10.1016/J.SBSPRO.2010.05.131.
[39] H.M. Wainwright, S. Finsterle, Y. Jung, Q. Zhou, J.T. Birkholzer, Making sense of global sensitivity analyses, Comput. Geosci. 65 (2014) 84–94, http://dx.doi.org/10.1016/J.CAGEO.2013.06.006.
[40] H. Rabitz, Ö.F. Aliş, J. Shorter, K. Shim, Efficient input—output model representations, Comput. Phys. Comm. 117 (1–2) (1999) 11–20, http://dx.doi.org/10.1016/S0010-4655(98)00152-0.
[41] I.M. Sobol, Global sensitivity indices for nonlinear mathematical models and their Monte Carlo estimates, Math. Comput. Simulation 55 (1–3) (2001) 271–280, http://dx.doi.org/10.1016/S0378-4754(00)00270-6.
[42] M.D. Morris, Factorial sampling plans for preliminary computational experiments, Technometrics 33 (2) (1991) 161–174, http://dx.doi.org/10.1080/00401706.1991.10484804, URL: https://www.tandfonline.com/doi/abs/10.1080/00401706.1991.10484804.
[43] A.-T. Nguyen, S. Reiter, A performance comparison of sensitivity analysis methods for building energy models, Build. Simul. 8 (6) (2015) 651–664, http://dx.doi.org/10.1007/s12273-015-0245-4.
[44] G. Li, C. Rosenthal, H. Rabitz, High dimensional model representations, J. Phys. Chem. A 105 (33) (2001) 7765–7777, http://dx.doi.org/10.1021/jp010450t.
[45] G. Li, S.-W. Wang, H. Rabitz, Practical approaches to construct RS-HDMR component functions, J. Phys. Chem. A 106 (37) (2002) 8721–8733, http://dx.doi.org/10.1021/jp014567t.
[46] G. Li, J. Hu, S.-W. Wang, P.G. Georgopoulos, J. Schoendorf, H. Rabitz, Random sampling-high dimensional model representation (RS-HDMR) and orthogonality of its different order component functions, J. Phys. Chem. A 110 (7) (2006) 2474–2485, http://dx.doi.org/10.1021/jp054148m.
[47] T. Ziehn, K.J. Hughes, J.F. Griffiths, R. Porter, A.S. Tomlin, A global sensitivity study of cyclohexane oxidation under low temperature fuel-rich conditions using HDMR methods, Combust. Theory Model. 13 (4) (2009) 589–605, http://dx.doi.org/10.1080/13647830902878398.
[48] T. Ishigami, T. Homma, An importance quantification technique in uncertainty analysis for computer models, in: Proceedings. First International Symposium on Uncertainty Modeling and Analysis, IEEE Comput. Soc. Press, 1990, pp. 398–403, http://dx.doi.org/10.1109/ISUMA.1990.151285.
[49] J. Herman, W. Usher, SALib: An open-source Python library for sensitivity analysis, J. Open Source Softw. 2 (9) (2017) 97, http://dx.doi.org/10.21105/joss.00097.
[50] K.-C. Chen, J.-Y. Lan, Y.-C. Tai, Description of local dilatancy and local rotation of granular assemblies by microstretch modeling, Int. J. Solids Struct. 46 (21) (2009) 3882–3893, http://dx.doi.org/10.1016/j.ijsolstr.2009.07.011.
[51] B. Soltanbeigi, A. Podlozhnyuk, C. Kloss, S. Pirker, J.Y. Ooi, S.-A. Papanicolopulos, Influence of various DEM shape representation methods on packing and shearing of granular assemblies, Granul. Matter 23 (2) (2021) 26, http://dx.doi.org/10.1007/s10035-020-01078-y.
[52] C.M. Wensrich, A. Katterfeld, Rolling friction as a technique for modelling particle shape in DEM, Powder Technol. 217 (2012) 409–417, http://dx.doi.org/10.1016/J.POWTEC.2011.10.057.
[53] N. Estrada, E. Azéma, F. Radjai, A. Taboada, Identification of rolling resistance as a shape parameter in sheared granular media, Phys. Rev. E 84 (1) (2011) 011306, http://dx.doi.org/10.1103/PhysRevE.84.011306.
[54] R.M. Nedderman, Statics and Kinematics of Granular Materials, Cambridge University Press, 1992, http://dx.doi.org/10.1017/CBO9780511600043.
[55] P. Artega, U. Tüzün, Flow of binary mixtures of equal-density granules in hoppers—size segregation, flowing density and discharge rates, Chem. Eng. Sci. 45 (1) (1990) 205–223, http://dx.doi.org/10.1016/0009-2509(90)87093-8.